Sub-pixel-scale Land Cover Map Updating by Integrating Change Detection and Sub-Pixel Mapping

Xiaodong Li, Yun Du, and Feng Ling

Abstract

Coarse-resolution remotely sensed images are high in temporal repetition rates, but their low spatial resolution limits their application in updating land cover maps. Our proposed land cover updating method involves the use of coarse-resolution images to update fine-resolution land cover maps. The method comprises change detection and sub-pixel mapping methods. The current coarse-resolution image is unmixed, and the previous fine-resolution map is spatially degraded to produce current and previous class fraction images. A change detection method is applied to these fraction images to create a fine-resolution binary change/non-change map. Finally, a sub-pixel mapping method is applied to update the fine-resolution pixel labels that are changed in the change/non-change map. The proposed method is compared with a pixel-based classification method and two sub-pixel mapping methods. The proposed method maintains most of the spatial patterns of land cover classes that are unchanged in the previous and current images, whereas other methods cannot.

Introduction

Remotely sensed images can provide reliable land cover information at different scales and are the primary data utilized in the production and updating of land cover maps. At the global scale, coarse-resolution images, such as those obtained with a moderate-resolution imaging spectroradiometer (MODIS), have been applied to build land cover products, such as the MODIS land cover product (Friedl *et al.*, 2002). Coarse-resolution images are high in temporal repetition rates, which allow the timely updating of land cover maps and the creation of long-term land cover products. However, the spatial resolution of coarse-resolution images is low. Coarse-resolution land cover products fail to satisfy regional-scale land cover resource and landscape analyses. At the regional scale, fine-resolution remotely sensed images are the primary data utilized to generate land cover maps. For instance, Landsat images at a spatial resolution of 30 m are utilized to produce and update the National Land Cover Database (NLCD) of the United States (Homer *et al.*, 2007). However, owing to the tradeoff between spatial and temporal resolution, fine-resolution images have their limitations because they are often acquired at a relatively low temporal resolution. The land cover products from fine-resolution images are derived only from remotely sensed data acquired during one or several years, and these products represent the land cover characteristics of a specific period. Therefore, they lack not only long-term but also timely land cover change information.

Using a current coarse-resolution image and a previous fine-resolution map to timely update fine-resolution land cover products at the regional scale is meaningful and challenging. This task necessitates the use of multi-resolution images, which provide mutually supplementary land cover information at different scales. A popular approach that combines fine-resolution and coarse-resolution images is the use of coarse-resolution images that cover the entire area as the primary data source, as well as fine-resolution images that cover a part of the area as training samples. Braswell *et al.* (2003) combined coarse-resolution and fine-resolution images to extract land cover fraction images at the sub-pixel scale using soft classification, which predicts land cover class fractional information within each coarse-resolution pixel. The fine-resolution images were utilized to train endmember signatures, and the coarse-resolution images were utilized for spectral unmixing. Lu *et al.* (2011) integrated MODIS and Landsat images to map a fractional forest cover in the Brazilian Amazon. MODIS images were unmixed to forest fraction images, whereas Landsat images were utilized to calibrate the forest fraction images. However, the aforementioned methods can only detect land cover fraction within each coarse-resolution pixel and cannot produce fine-resolution land cover maps.

Sub-pixel mapping (SPM) or super-resolution mapping is a technique that transforms a coarse-resolution image or a spectral unmixing result into a fine-scale hard classification map by dividing pixels into sub-pixels and assigning different classes to these sub-pixels (Foody, 2006; Atkinson, 2009). SPM provides more information than spectral unmixing during the downscaling of coarse-resolution images because SPM can specify the location of each class within the coarse pixels. Generally, SPM adopts mono-temporal coarse-resolution remotely sensed images as input. In fact, SPM is an ill-posed inverse problem of transforming a coarse-resolution fraction image to a fine-resolution land cover map, and SPM accuracy is influenced by the uncertainty in determining fine-resolution pixel labels (Nguyen *et al.*, 2006; Ling *et al.*, 2010). The combination of a current coarse-resolution image and a previous fine-resolution land cover map is useful in reducing SPM uncertainty. Ling *et al.* (2011) developed a sub-pixel scale land cover change mapping method by using a current coarse-resolution remotely sensed image and a previous fine-resolution land cover map. This method was directly used on land cover fraction images obtained by spectral unmixing applied to remotely sensed images; fraction image errors reduced the accuracy of the result.

The integration of a previous fine-resolution land cover map into land cover classification and map updating accuracy

Institute of Geodesy and Geophysics, Chinese Academy of sciences, 340 XuDong Rd. Wuhan 430077, Hubei, China (lingf@whigg.ac.cn).

Photogrammetric Engineering & Remote Sensing
Vol. 81, No. 1, January 2015, pp. 59–67.
0099-1112/15/811–59

doi: 10.14358/PERS.81.1.59

has been developed in recent years. Previous studies have shown that pixel-based classification methods that integrate previous land cover map information outperform methods that independently classify images. Xian *et al.* (2010) updated 2001 NLCD impervious surface products to 2006 through a change detection method with Landsat imagery. Chen *et al.* (2012) proposed an automatic approach to update land cover maps. With the application of a change detection method to the previous map and current image (Chen *et al.*, 2011), the aforementioned land cover map updating approaches are simplified to update only the labels of changed pixels in the current image. However, these methods require that current remotely sensed images have a spatial resolution as fine as that of the previous land cover map and that the advantage of coarse-resolution images with a high temporal resolution be ignored.

This study proposes a novel land cover map updating method that involves the use of a current coarse-resolution image and a previous fine-resolution land cover map to update fine-resolution land cover maps. The proposed method comprises a change detection method and an SPM method. The change detection method is utilized to detect which fine-resolution pixels are changed in each coarse-resolution image pixel, whereas SPM is used to label only the changed fine-resolution pixels instead of all the fine-resolution pixels in the image. The proposed method was validated on the basis of synthetic multi-spectral and Landsat images by comparison of the proposed method with a hard classification method and two SPM methods.

Methods

The proposed method comprises a change detection method and an SPM method. The change detection method is used to produce a fine-resolution binary change/non-change map. SPM is utilized to label only the changed fine-resolution pixels according to the binary change/non-change map.

Change Detection Method

Change detection techniques can be grouped into two categories. One category involves detecting binary change/non-change information, and the other category involves detecting the "from - to" change trajectory. In this study, fine-resolution pixel change/non-change information is detected on the basis of coarse- and fine-resolution images. Although several remote sensing techniques have been successfully used in change detection, most of them focus on the change "between" classes measured in a crisp way through which each pixel label is changed or unchanged in different images. When the spatial resolution of a remotely sensed pixel is coarse, the pixel is usually not pure and comprises different land cover classes. Therefore, crisp change detection methods are inappropriate for coarse-resolution image change detection. Rather, the significance arises in the way that land cover fractions within each pixel may change in different images. Spectral unmixing applied to coarse-resolution images can generate land cover fraction images that represent land-cover area proportions within each pixel at the sub-pixel scale. Fraction image-based change detection methods quantify the change in different classes within each pixel by comparing the fraction images acquired at different times, so these methods are suitable for the change detection of coarse-resolution remotely sensed images (Lu *et al.*, 2004a). In this study, the fraction image-based change detection method is applied to detect sub-pixel land cover change information by comparing a pair of current and previous fraction images.

Current fraction images are produced by applying spectral unmixing to the current coarse-resolution image. Previous studies have confirmed that linear spectral mixture analysis (LSMA) can extract land cover fractions that represent area proportions of the endmembers within the pixel and can be applied in land cover fractional change detection (Roberts *et al.*,1998; Ju *et al.*, 2003; Lu *et al.*, 2004b). In this study, LSMA is applied to current coarse-resolution images to generate current land cover fraction images.

The previous coarse-resolution fraction images are spatially degraded on the basis of the previous fine-resolution land cover map with the use of a mean filter (Foody *et al.*, 2002; Tatem *et al.*, 2003; Wang *et al.*, 2014). We assume C classes in the previous map. C fine-resolution binary category maps are first produced. In the k^{th} ($k = 1, \ldots, C$) fine-resolution land cover category map, a value of 1 is assigned to the fine-resolution pixel if it belongs to class k; otherwise, a value of 0 is assigned to it. The scale factor between the size of the coarse-resolution image pixel and the pixel in the fine-resolution map is defined as s, and each coarse-resolution pixel contains s^2 fine-resolution pixels (sub-pixels). Each of the C fine-resolution binary category maps is then spatially degraded with a mean filter that has an $s \times s$ fine-resolution pixel window to generate a previous coarse-resolution fraction image of that class.

After the current and previous coarse-resolution fraction images are produced, the change/non-change information of each class in every coarse-resolution pixel can be obtained. A fraction differencing image for each class is produced by application of a subtraction operation to the current and previous fraction images of that class. Assume that $F_{k,pre}$ and $F_{k,cur}$ are the previous and current fraction images of class k. ΔF_k is the fraction differencing image of class k and is calculated as follows:

$$\Delta F_k = F_{k,pre} - F_{k,cur} . \quad (1)$$

In implementing change/non-change detection on each fraction differencing image, establishing a threshold level to define the land cover change of that class in each coarse-resolution pixel is necessary. In this study, the threshold is determined through the use of training images (Lu *et al.*, 2004b). These training images include a pair of a previous fine-resolution map and a current coarse-resolution remotely sensed image of a training region. The previous training image is acquired temporally close to the previous data as the input of proposed model, and the current training image is acquired temporally close to the current data as the input of proposed model. The previous fine-resolution training map is spatially degraded into the previous training fraction images, and the current coarse-resolution training image is unmixed into the current training fraction images. The training fraction differencing images are obtained from the pair of previous and current training fraction images according to Equation 1. The selection of thresholds for each class is based on statistical analysis of unchanged land-cover sample plots within the training fraction differencing image of that class, in consideration of the fact that unchanged land covers have normally distributed histograms in fraction differencing values (the mean value is close to zero), whereas changed land covers do not. Assume that SD_k is the standard deviation of the values of pixels that cover the unchanged sample plots in the training fraction differencing image of class k. The land cover fraction change/non-change threshold value for class k, called T_k, equals to $3 \times SD_k$ (Lu *et al.*, 2004b).

The fine-resolution binary change/non-change map is created after the fraction change/non-change threshold for each class is determined with the use of the training data. The change or non-change of each fine-resolution pixel is determined as follows. We assume that b_i is the i^{th} coarse-resolution pixel in the current image, and $a_{i,j}$ is the j^{th} fine-resolution pixel in b_i. We also assume that the label of $a_{i,j}$ in the previous map is class k. First, we determine whether the fraction value of class k in b_i is changed by comparing the value of coarse-resolution i in the fraction differencing image

ΔF_k (called $\Delta F_{k,i}$) and the threshold value T_k. If $\Delta F_{k,i}$ falls in the range of $-T_k$ to T_k, the fraction value of class k in b_i is unchanged; otherwise, the fraction value of class k in b_i is changed. We make the simple assumption that if the fraction value of class k in b_i is unchanged, then all the fine-resolution pixels labeled as class k in b_i in the previous map are unchanged; therefore, the fine-resolution pixel $a_{i,j}$ is labeled as "unchanged" in the fine-resolution binary change/non-change map. Likewise, if the fraction value of class k in b_i is changed, all the fine-resolution pixels labeled as class k in b_i in the previous map are changed, and the fine-resolution pixel $a_{i,j}$ is labeled as "changed" in the fine-resolution binary change/non-change map.

Sub-pixel Mapping

SPM is an approach to predict fine-resolution pixel (or sub-pixel) labels within each coarse-resolution pixel. SPM is essentially a hard classification technique at a finer spatial resolution than that of the input coarse-resolution remotely sensed image. Several SPM methods have been proposed in recent years (Table 1). These methods include pixel-swapping algorithm (Atkinson, 2005; Foody and Doan, 2007; Makido *et al.*, 2007; Li *et al.*, 2011; Tong *et al.*, 2013; Xu and Huang, 2014), Hopfield neural networks (Tatem *et al.*, 2003; Ling *et al.*, 2010; Muad and Foody, 2012), spatial attraction model (Mertens *et al.*, 2006; Ge *et al.*, 2009; Shen *et al.*, 2009; Ling *et al.*, 2013), Markov random field (Kasetkasem *et al.*, 2005; Tolpekin and Stein, 2009; Ardila *et al.*, 2011; Li *et al.*, 2012; Wang and Wang, 2013), spatial-spectral managed model (Ling *et al.*, 2012; Li *et al.*, 2014), spatial regularization (Villa *et al.*, 2011), indicator kriging (Boucher and Kyriakidis, 2007; Wang *et al.*, 2014), interpolation model (Ling et al., 2013), multiple-point simulating model (Ge, 2013), particle swarm optimization (Wang *et al.*, 2012), and supervised fuzzy c-means-based model (Li *et al.*, 2012).

Spatial-spectral managed SPM algorithm (SSMA) is a simple yet effective method that can be applied directly to remotely sensed images. SSMA is utilized in this study to label current fine-resolution pixels marked as changed pixels in the fine-resolution change/non-change map, rather than labeling all current fine-resolution pixel labels in the entire image as traditional SPM methods do. SSMA comprises three parts: a spatial term, a spectral term, and a balance parameter. The spatial term is the regularization term aiming to make the solution smooth. The spectral term is the data term to preserve information of the original coarse-resolution image. The balance parameter is utilized to balance the contribution of the spatial and spectral terms.

We assume that the coarse-resolution image is **y**, and **y** contains B bands with each band containing n pixels. The output of SPM is a fine-resolution land cover map (**c**). The goal function (E) of SSMA is characterized as:

$$E = \lambda \cdot E^{spatial} + E^{spectral} \tag{2}$$

where $E^{spatial}$ is the spatial term, $E^{spectral}$ is the spectral term, and λ is the balance parameter.

The SSMA spatial term aims to maximize the spatial correlation of neighboring fine-resolution pixels based on the assumption that spatially proximate observations of a given property are more similar than distant observations (Verhoeye and De Wulf, 2002; Makido and Shortridge, 2007; Atkinson, 2009). The spatial term for fine-resolution pixel j in coarse-resolution pixel i, $a_{i,j}$, is computed as:

$$E^{spatial}\left(c(a_{i,j})\right) = \sum_{l \in N(a_{i,j})} \frac{1}{d\left(a_{i,j}, a_l\right)} \cdot \delta\left(c(a_{i,j}), c(a_l)\right) \tag{3}$$

where $N(a_{i,j})$ is a symmetric neighborhood system that includes all fine-resolution pixels inside a square window whose center is $a_{i,j}$ ($a_{i,j}$ itself is not included in the window); $d(a_{i,j}, a_l)$ is the Euclidian distance between $a_{i,j}$ and $a_l (a_l \in N(a_{i,j}))$; $c(a_{i,j})$ and $c(a_l)$ are the land cover class labels of fine-resolution pixels a_i and a_l. $\delta(c(a_{i,j}), c(a_l))$ is defined as:

$$\delta\left(c(a_{i,j}), c(a_l)\right) = \begin{cases} -1 & c(a_l) = c(a_{i,j}) \\ 0 & c(a_l) \neq c(a_{i,j}) \end{cases}. \tag{4}$$

The spectral term is utilized to preserve information of the original coarse-resolution image. Assume that $\boldsymbol{y}_i$ is the observed pixel spectral value of pixel b_i in **y**, $\boldsymbol{\mu}_i$ is the synthetic coarse-resolution pixel spectral vector of pixel b_i. Assume that the spectrum measured by a sensor is a linear combination of the spectra of all components within the pixel, $\boldsymbol{\mu}_i$ is calculated as:

$$\boldsymbol{\mu}_i = \sum_{k=1}^{C} \theta_{ki} \boldsymbol{\mu}_k \tag{5}$$

where θ_{ki} is the proportion of class k in pixel b_i; θ_{ki} is calculated from label map **c** which is the SSMA intermediate result in each iteration, by dividing the number of fine-resolution

Table 1. Sub-Pixel Mapping (SPM) Method Names and Important Mathematical Variables Definition

SPM and variables names	Definition
PSA	Pixel-swapping algorithm based SPM
SSMA	Spatial–spectral managed SPM
CD_SSMA	Land cover map updating method that incorporates change detection and SSMA
MDC	Minimum distance classifier
y	Current coarse-resolution image
c	Current fine-resolution land cover map outputted from SPM
ΔF_k	Fraction differencing image of class k
T_k	Land cover fraction change/non-change threshold value for class k in ΔF_k
b_i	The i-th coarse-resolution pixel in the current image
$a_{i,j}$	The j-th fine-resolution pixel in b_i.
$c(a_{i,j})$	The land cover class label of the fine-resolution pixel $a_{i,j}$
s	Scale factor between the size of the coarse-resolution image pixel and the pixel in the fine-resolution map
λ	Balance parameter in SSMA and CD_SSMA

pixels labeled as class k in pixel b_i by total fine-resolution pixel number, i.e., s^2, in b_i; and $\boldsymbol{\mu}_k$ is the endmember spectral vector of class k. The SSMA spectral term for pixel b_i is expressed as

$$E^{spectral}(b_i) = (\mathbf{y}_i - \boldsymbol{\mu}_i)^T(\mathbf{y}_i - \boldsymbol{\mu}_i) \quad (6)$$

where T is the transposition operation. Therefore, the goal function (E) of SSMA is calculated as:

$$E = \lambda \cdot \sum_{i,j} E^{spatial}\left(c(a_{i,j})\right) + \sum_{i} E^{spectral}\left(b_i\right) \quad . \quad (7)$$

SSMA optimization is achieved by minimizing the goal function through simulated annealing (Geman and Geman, 1984).

Land Cover Map Updating by Integrating Change Detection and SPM

The proposed land cover map updating method that incorporates change detection and SSMA (CD_SSMA) is a modification of SSMA. Compared with SSMA, CD_SSMA adopts the fine-resolution binary change/non-change map and the previous fine-resolution map as base maps to update the fine-resolution pixel labels. CD_SSMA determines if the fine-resolution pixel is changed before labeling this fine-resolution pixel. If a fine-resolution pixel is detected as "changed" in the binary change/non-change map, this fine-resolution pixel is labeled according to the SSMA goal function; if a fine-resolution pixel is detected as "unchanged" in the binary change/non-change map, this fine-resolution pixel is labeled according to the previous fine-resolution land cover map. The flowchart of CD_SSMA is shown in Figure 1.

Methods for Comparison

CD_SSMA was compared with a hard classification method and two SPM methods. Minimum distance classifier (MDC) was employed as the hard classification method to generate the pixel-based classification map. The pixel-swapping algorithm (PSA) (Atkinson, 2005) and SSMA were utilized as SPM methods for comparison. PSA is a widely used SPM method. In the PSA initialization step, the fine-resolution pixels of each class within each coarse-resolution pixel are randomly labeled according to the numbers calculated with the use of land cover fraction images, which are the output of a spectral unmixing model. In each iteration, two fine-resolution pixels with different land cover labels are randomly selected from each coarse-resolution pixel. If swapping these two fine-resolution pixels increases the land cover spatial dependence of the land cover map, these two fine-resolution pixels are swapped. PSA stops when a fixed number of iteration is reached. MDC, PSA, and SSMA adopt a coarse-resolution mono-temporal image as input.

Experimental Results

Experiment on Synthetic Multi-spectral Images

A synthetic multi-spectral image was used as the current coarse-resolution image to avoid spectral signature bias in deriving the endmember signatures. The previous and current

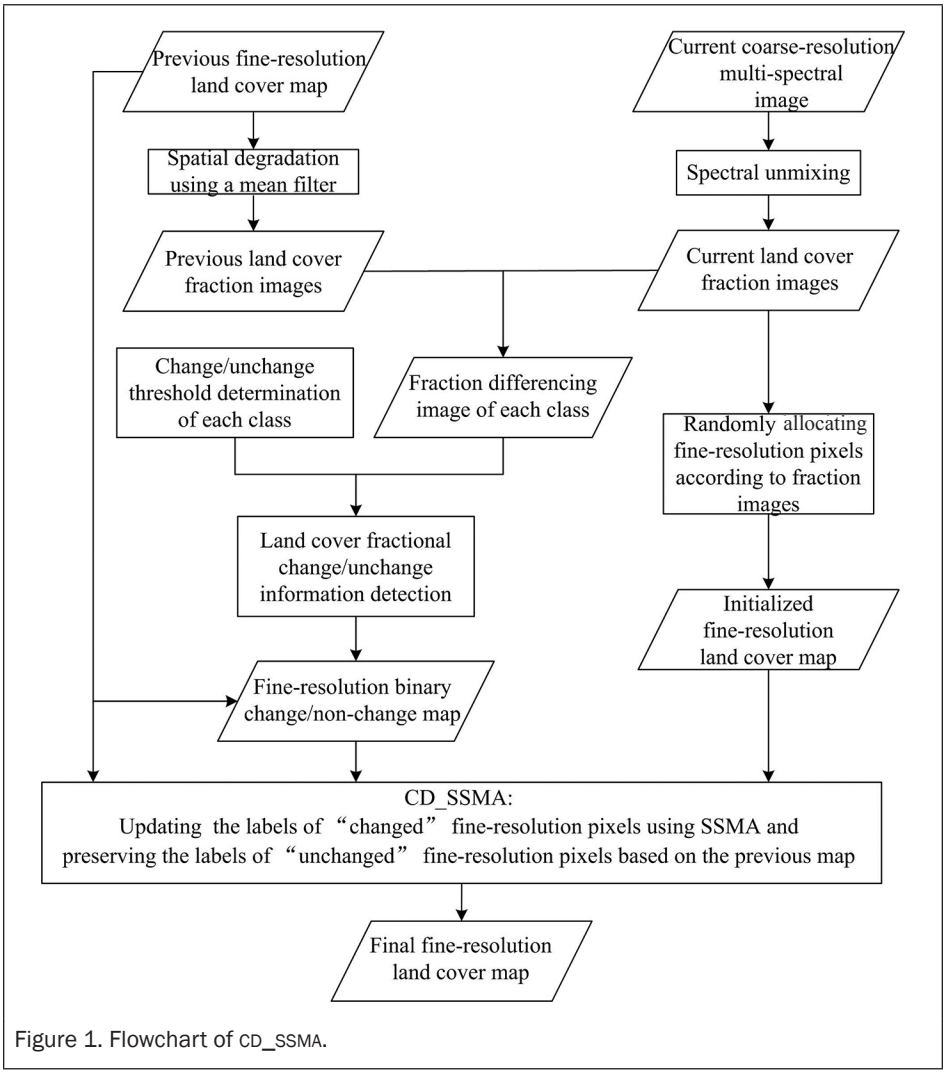

Figure 1. Flowchart of CD_SSMA.

fine-resolution land cover maps were obtained from NLCD 2001 and 2006, respectively. NLCD is a land cover classification scheme that has been applied consistently at a spatial resolution of 30 m across the United States. NLCD is based primarily on unsupervised classification of Landsat satellite data. NLCD 2001 and 2006 are strictly geo-registered to the Albers Equal Area projection grid (Homer *et al.*, 2004). In this study, the original 16 land cover classes in NLCD 2001 and 2006 were combined and reclassified into five classes, namely, Water-Wetlands, Developed-Barren, Forest, Shrubland-Herbaceous, and Planted/Cultivated.

Both the previous map obtained from NLCD2001 and the current map obtained from NLCD2006 contain 800 × 800 pixels of the same area located in Charlotte, North Carolina. The previous map is used as CD_SSMA input. The current map is used not only as the reference map for model validation, but also to produce the current coarse-resolution multi-spectral image. The number of bands was set to 4 to simulate the fine-resolution multi-spectral images. The five endmember signature DN values were set to $[380, 490, 300, 320]^T$, $[310, 335, 235, 260]^T$, $[250, 410, 180, 390]^T$, $[230, 360, 320, 345]^T$, and $[450, 220, 120, 170]^T$. The spectral response of each class was assumed to be normally distributed in each waveband. The covariance matrixes for all the classes were set to $600 \cdot \mathbf{M}$, where $\mathbf{M}$ is a 4 × 4 matrix of 1. The coarse-resolution multi-spectral images were then generated by spatially degrading the fine-resolution multi-spectral image with a mean filter with scale factor $s = 5$ and $s = 10$ (Tolpekin and Stein, 2009).

The training images used to determine the land cover fraction change/non-change threshold values were also obtained from NLCD2001 and NLCD2006. The previous and current fine-resolution training maps contain 4,000 × 4,000 pixels near the study area. The current coarse-resolution multi-spectral image was produced on the basis of the current fine-resolution training map with the use of the same method as that used to produce the multi-spectral testing data as CD_SSMA input.

The parameters of the different SPM methods were set. Neighborhood window size, which is the length of the square side of the neighborhood, was set to 5 in PSA (Makido and Shortridge, 2007) and 7 in both SSMA and CD_SSMA (Ardila *et al.*, 2011). Balance parameter λ in SSMA and CD_SSMA was set empirically. If λ is small, the result maps are unsmoothed with isolated patches; if λ is large, the result maps are oversmoothed with rounded patches. In this study, $\lambda = 80$ was set at $s = 5$, and $\lambda = 5$ was set at $s = 10$.

The CD_SSMA training images are shown in Plate 1. A mean filter was used to spatially degrade the previous fine-resolution training map. LSMA was utilized to unmix the current coarse-resolution training image. Comparing the previous and current fraction images obtained from the training images and applying the supervised change detection method (Lu *et al.*, 2004b) to the images helped determine the land cover fraction change/non-change threshold values of the fractional change for each class (Table 2).

Plate 1 also shows the classification and SPM results, which differ significantly. The class boundaries in the MDC result are serrated and rough because the hard classification map is produced at the pixel scale and the mixed pixels are labeled as monotypes regardless of the spatial patterns of land cover classes within mixed pixels. In the PSA and SSMA results, the land cover patches are aggregated into rounded patches because SPM maximizes the spatial correlation of neighboring fine-resolution pixels. Many speckle artifacts in salt-and-pepper appearance can be seen in the PSA result. This is because the fine-resolution pixel number of a class, which is determined by class fractions of that class in the coarse-resolution pixel, is very few, and these fine-resolution pixels are characterized as speckle artifacts in the result map. In PSA, swapping a pair of fine-resolution pixels within the coarse-resolution pixel does not change class fractions. By contrast, such speckle artifacts are mostly eliminated by SSMA in which the land cover fractions can be changed before and after SPM (Kasetkasem *et al.*, 2005; Tolpekin and Stein, 2009; Ling *et al.*, 2012; Li *et al.*, 2014). The CD_SSMA result matches the reference map better than the other results. The speckle artifacts are eliminated, and the spatial pattern of the linear-shaped Developed-Barren class, which is unchanged in the previous and current maps, is preserved in the zoomed area because CD_SSMA incorporates a change detection method and preserves the unchanged fine-resolution pixel labels. The scale factor plays an important role in the results. With the increase in the scale factor, the MDC map becomes coarse and the PSA and SSMA maps acquire more aggregated patches. By contrast, the CD_SSMA result does not change significantly.

Table 2. Land Cover Fraction Change/Non-Change Threshold Values for Different Classes for Synthetic Images

		s=5	s=10
Threshold value	Water-Wetlands	0.1043	0.0612
	Developed-Barren	0.1995	0.1301
	Forest	0.0432	0.0290
	Shrubland-Herbaceous	0.0835	0.0543
	Planted/Cultivated	0.0618	0.0473

Table 3. Accuracies of the Different Methods Using Synthetic Images

		Kappa	QD	AD	OA
S = 5	MDC	0.6753	0.0289	0.2050	0.7806
	PSA	0.7071	0.0080	0.2055	0.8008
	SSMA	0.7200	0.0390	0.1619	0.8110
	CD_SSMA	0.9172	0.0088	0.0513	0.9507
S = 10	MDC	0.5336	0.0535	0.2660	0.7004
	PSA	0.5188	0.0094	0.3442	0.6747
	SSMA	0.5527	0.0211	0.3016	0.6997
	CD_SSMA	0.7774	0.0103	0.1514	0.8575

A quantitative comparison was conducted with Kappa value, quantitative disagreement (QD), and allocation disagreement (AD) to assess the match between the reference land cover map and the resulting land cover map. QD is the difference between the reference and resulting maps caused by a less-than-optimal match in the proportions of categories. AD is the difference between the reference and resulting maps caused by a less-than-optimal match in the spatial allocation of categories given the proportions of the categories in the reference and resulting maps. Low values of QD and AD show a good match between the resulting and reference maps (Pontius and Millones, 2011). Overall accuracy (OA) calculated from the change/non-change matrix was utilized to quantify the match between the real change/non-change map and the resulting change/non-change map. The real change/non-change map is produced by a per-pixel comparison of the reference and previous maps, whereas the resulting change/non-change map is produced by a per-pixel comparison of the resulting and previous maps. The accuracies of the different methods are shown in Table 3. The Kappa and OA values for all the methods are higher at $s = 5$ than at $s = 10$, and the QD and AD values for all the methods are lower at $s = 5$ than at $s = 10$ except for the QD value for SSMA. This result shows that coarsening the current coarse-resolution remotely sensed image always reduces the accuracy of different methods in land cover map updates. The Kappa values of CD_SSMA are approximately 0.20 higher than

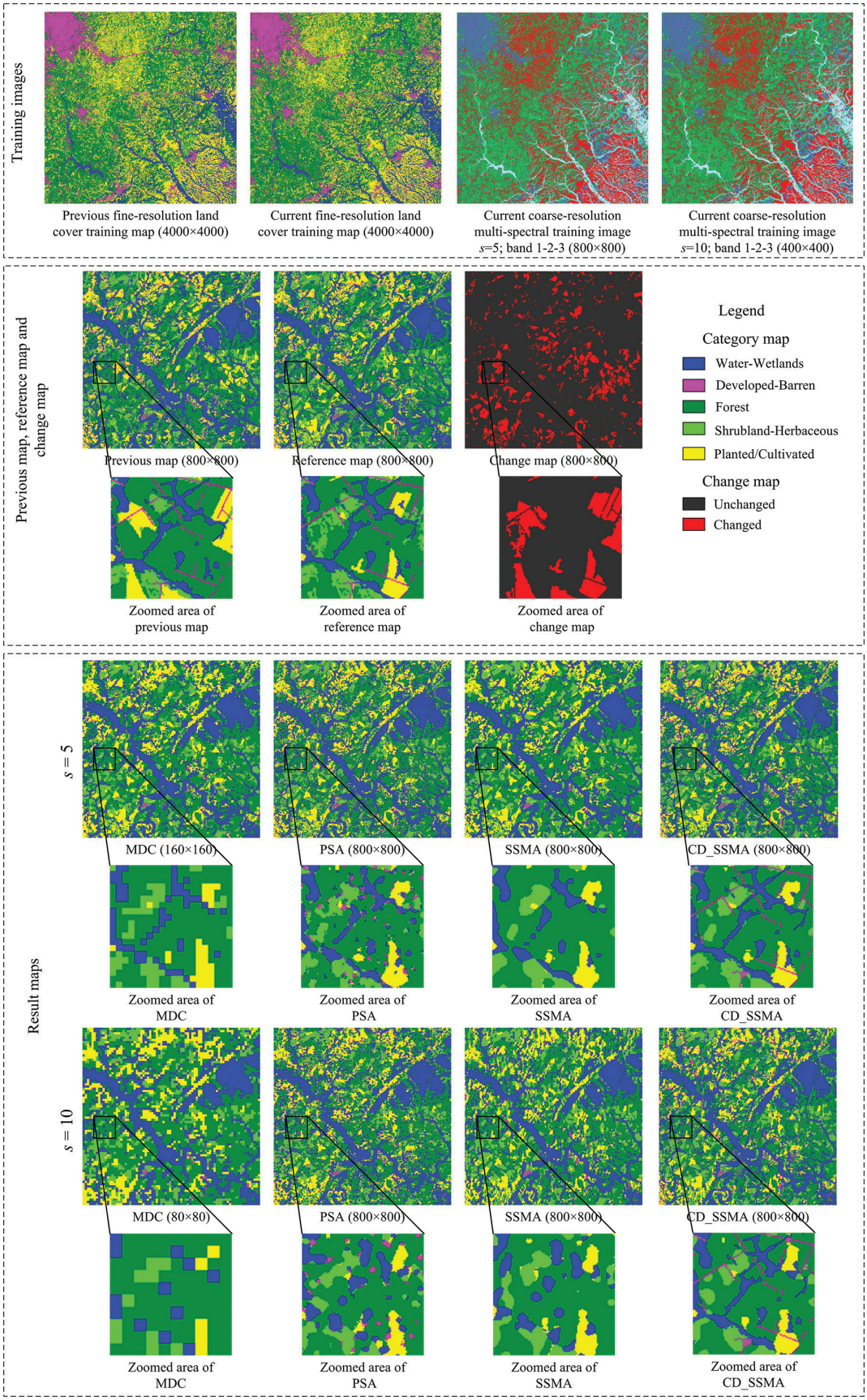

Plate 1. Training images, previous map, reference map, change map, and result maps of different methods using a synthetic multi-spectral image: (a) Training images, (b) Previous map, reference map, and change map, and (c) Results map.

those of the other methods, and the OA values of CD_SSMA are approximately 0.15 higher than those of the other methods at $s = 5$ and $s = 10$. The QD and AD values for MDC are high; this finding reveals the influence of the mixed pixel problem on pixel-based classification. The AD value for PSA is extremely high; this result shows that the uncertainty of the spatial locations of different land cover classes is the main factor that affects accuracy. The QD and AD values for CD_SSMA are lower than those of SSMA, MDC, and PSA at $s = 5$ and $s = 10$ (except for the QD value of PSA). Thus, CD_SSMA is effective to predict the locations of land cover classes at the sub-pixel scale.

Experiment on Landsat Images

CD_SSMA was validated on Landsat multi-spectral imageries in this experiment. The study area is located near Sorriso (12°33'21"S and 55°42'31"W) in Mato Grosso State, Brazil. This area is in the Brazilian Amazon Basin, which is mainly covered by tropical forests and has undergone a massive deforestation process in recent years. A Thematic Mapper (TM) image acquired on 11 July 1988 with a spatial resolution of 28.5 m was employed to produce the previous land cover map. A Landsat Enhanced Thematic Mapper+ (ETM+) image acquired on 18 July 2005 with a spatial resolution of 30 m was utilized to produce the reference land cover map. The TM

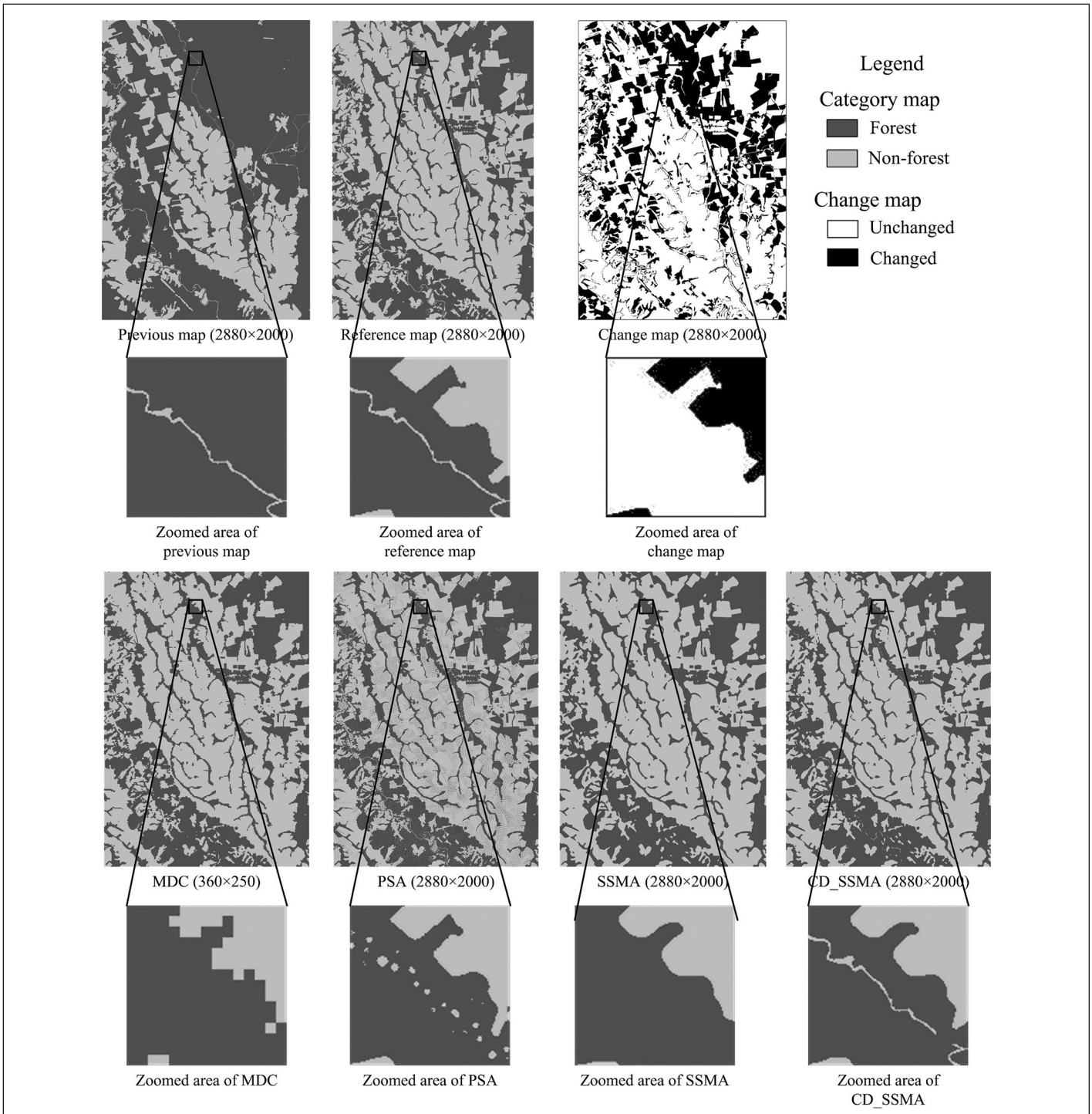

Figure 2. SPM and classification results of different methods using Landsat images.

image was geo-registered to the ETM+ image and resampled at a spatial resolution of 30 m. The registration error between the TM and ETM+ images was less than 0.5 pixel. The TM and ETM+ images were subset with 2,880 × 2,000 pixels and then manually digitized to the previous and reference maps with forest and non-forest classes in the maps. In addition, the ETM+ image (red and near-infrared bands) was spatially degraded into the coarse-resolution image with a mean filter with the scale factor $s = 8$ to simulate the first two bands of MODIS image at a spatial resolution of 250 m.

The previous and current fine-resolution training images with 1,600 × 1,600 fine-resolution pixels were obtained from the same TM and ETM+ images located near the study area. The previous fine-resolution training image was manually digitized to the previous training land cover map, which was then spatially degraded into the previous fraction images with a mean filter at $s = 8$. The current fine-resolution training image was spatially degraded into the coarse-resolution multi-spectral images with a mean filter at $s = 8$, which was then unmixed into current fraction images with the use of LSMA. Comparison of the pair of previous and current training fraction images with the use of the supervised change detection method (Lu *et al.*, 2004b) shows that the land cover fraction change/non-change threshold values were 0.1585 for both forest and non-forest. The neighborhood window size values in PSA, SSMA, and CD_SSMA were set similar to those in the synthetic image experiment. $\lambda = 1$ was set in SSMA and CD_SSMA through numerous trials.

As can be seen in Figure 2, MDC generates aggregated and discontinuous patches. The small linear object in the zoomed area is eliminated because of the coarse resolution of the remotely sensed image. In the PSA result, the linear object is discontinuous. In the SSMA result, the linear object is eliminated because of the spatial smoothing effect. By contrast, the linear object is mostly preserved in the CD_SSMA result. Quantitative analysis shows that the Kappa and OA values of CD_SSMA are higher than those of other methods (Table 4). Although the QD value of CD_SSMA is approximately 0.003 higher than that of MDC and SSMA, the AD value of CD_SSMA is approximately 0.01 lower than that of the other methods.

Table 4. Accuracies of the Different Methods Using Landsat Images

	Kappa	QD	AD	OA
MDC	0.8862	0.0147	0.0429	0.9524
PSA	0.8890	0.0203	0.0326	0.9471
SSMA	0.8993	0.0142	0.0336	0.9522
CD_SSMA	0.9116	0.0181	0.0239	0.9570

Conclusions

CD_SSMA, a sub-pixel scale land cover map updating method that integrates change detection and SPM, was developed in this study. CD_SSMA utilizes current coarse-resolution images with high temporal resolution and previous land cover maps with fine spatial resolution to update land cover maps with high temporal and fine spatial resolutions. Unlike other SPM methods that directly label all the fine-resolution pixels in the image, CD_SSMA employs a change detection method to produce a fine-resolution binary change/non-change map and only updates the fine-resolution pixels that are changed in the binary change/non-change map through the use of SSMA. The spatial patterns of the unchanged fine-resolution pixels in the previous map can be preserved in the CD_SSMA result.

The proposed method was tested on synthetic multi-spectral and Landsat images by comparing the proposed method with a hard classification method and two SPM methods, namely, PSA and SSMA. The results show that the hard classification method generates land cover maps with serrated boundaries because of the coarse resolution of the remotely sensed image. PSA generates land cover maps with speckle artifacts, and SSMA generates land cover maps with over-smoothed boundaries. CD_SSMA generates land cover maps that are close to the reference map and preserves most of the spatial patterns of the unchanged classes. Quantitative analysis shows that the CD_SSMA results have higher Kappa values and lower allocation disagreement values in all experiments by comparison with the results of the other methods.

The accuracy of CD_SSMA is related to the number of constraints. First, CD_SSMA requires that the registration error between the previous fine-resolution land cover map and the current coarse-resolution image be strictly controlled because mis-registration will reduce the change detection accuracy. Furthermore, training images are necessary to obtain the threshold value for the identification of unchanged classes in every coarse-resolution pixel. Unsupervised threshold determination methods that can be applied without image training must be developed. Finally, the balance parameter in the SPM procedure of CD_SSMA was set by trials. A comprehensive study that involves the automatic estimation of the optimal balance parameter value is required in the future.

Acknowledgments

This work was supported in part by the Natural Science Foundation of China under Grant No. 41301398, in part by the National Basic Research Program (973 Program) of China under Grant No. 2013cb733205 and in part by Natural Science Foundation of Hubei Province for Distinguished Young Scholars under Grant No. 2013CFA031.

References

Ardila, J.P., V.A. Tolpekin, W. Bijker, and A. Stein, 2011. Markov-random-field-based super-resolution mapping for identification of urban trees in VHR images, *ISPRS Journal of Photogrammetry and Remote Sensing*, 66(6):762–775.

Atkinson, P.M., 2005. Sub-pixel target mapping from soft-classified, remotely sensed imagery, *Photogrammetric Engineering & Remote Sensing*, 71(7):839–846.

Atkinson, P.M., 2009. Issues of uncertainty in super-resolution mapping and their implications for the design of an inter-comparison study, *International Journal of Remote Sensing*, 30(20):5293–5308.

Boucher, A., and P.C. Kyriakidis, 2007. Integrating fine scale information in super-resolution land-cover mapping, *Photogrammetric Engineering & Remote Sensing*, 73(8):913–921.

Braswell, B.H., S.C. Hagen, S.E. Frolking, and W.A. Salas, 2003. A multivariable approach for mapping sub-pixel land cover distributions using MISR and MODIS: Application in the Brazilian Amazon region, *Remote Sensing of Environment*, 87(2-3):243–256.

Chen, J., X. Chen, and X. Cui, 2011. Change vector analysis in posterior probability space: A new method for land cover change detection, *IEEE Geoscience and Remote Sensing Letters*, 8(2):317–321.

Chen, X., J. Chen, Y. Shi, and Y. Yamaguchi, 2012. An automated approach for updating land cover maps based on integrated change detection and classification methods, *ISPRS Journal of Photogrammetry and Remote Sensing*, 71:86–95.

Congalton, R.G., 1991. A review of assessing the accuracy of classifications of remotely sensed data, *Remote Sensing of Environment*, 37(1):35–46.

Foody, G.M., 2006. Sub-pixel methods in remote sensing, *Remote Sensing Image Analysis: Including the Spatial Domain*, pp. 37–49.

Foody, G.M., and H.T.X. Doan, 2007. Variability in soft classification prediction and its implications for sub-pixel scale change detection and super resolution mapping, *Photogrammetric Engineering & Remote Sensing*, 73(8):923–933.

Foody, G.M., P.M. Atkinson, and J. Wiley, 2002. *Uncertainty in Remote Sensing and GIS*, Wiley Online Library.

Friedl, M.A., D.K. McIver, J.C. Hodges, X. Zhang, D. Muchoney, A.H. Strahler, C.E. Woodcock, S. Gopal, A. Schneider, and A. Cooper, 2002. Global land cover mapping from MODIS: Algorithms and early results, *Remote Sensing of Environment*, 83(1):287–302.

Ge, Y., 2013. Sub-pixel land-cover mapping with improved fraction images upon multiple-point simulation, *International Journal of Applied Earth Observation and Geoinformation*, 22:115–126.

Ge, Y., S. Li, and V.C. Lakhan, 2009. Development and testing of a sub-pixel mapping algorithm, *IEEE Transactions on Geoscience and Remote Sensing*, 47(7):2155–2164.

Geman, S., and D. Geman, 1984. Stochastic relaxation, Gibbs distributions, and the Bayesian restoration of images, *IEEE Transactions on Pattern Analysis and Machine Intelligence*, 6(6):721–741.

Homer, C., C. Huang, L. Yang, B. Wylie, and M. Coan, 2004. Development of a 2001 National Land-Cover Database for the United States, *Photogrammetric Engineering & Remote Sensing*, 70(7):829–840.

Homer, C., J. Dewitz, J. Fry, M. Coan, N. Hossain, C. Larson, N. Herold, A. McKerrow, J.N. VanDriel, and J. Wickham, 2007. Completion of the 2001 National Land Cover Database for the conterminous United States, *Photogrammetric Engineering & Remote Sensing*, 73(4):337–341.

Ju, J., E.D. Kolaczyk, and S. Gopal, 2003. Gaussian mixture discriminant analysis and sub-pixel land cover characterization in remote sensing, *Remote Sensing of Environment*, 84(4):550–560.

Kasetkasem, T., M.K. Arora, and P.K. Varshney, 2005. Super-resolution land cover mapping using a Markov random field based approach, *Remote Sensing of Environment*, 96(3-4):302–314.

Li, X., F. Ling, and Y. Du, 2012. Super-resolution mapping based on the supervised fuzzy c-means approach, *Remote Sensing Letters*, 3(6):501–510.

Li, X., Y. Du, and F. Ling, 2012. Spatially adaptive smoothing parameter selection for Markov random field based sub-pixel mapping of remotely sensed images, *International Journal of Remote Sensing*, 33(24):7886–7901.

Li, X., F. Ling, Y. Du, and Y. Zhang, 2014. Spatially adaptive superresolution land cover mapping with multispectral and panchromatic images, *IEEE Transactions on Geoscience and Remote Sensing*, 52(5):2810–2823.

Li, X., Y. Du, F. Ling, S. Wu, and Q. Feng, 2011. Using a sub-pixel mapping model to improve the accuracy of landscape pattern indices, *Ecological Indicators,* 11(5):1160–1170.

Ling, F., W. Li, Y. Du, and X. Li, 2011. Land cover change mapping at the subpixel scale with different spatial-resolution remotely sensed imagery, *IEEE Geoscience and Remote Sensing Letters*, 8(1):182–186.

Ling, F., Y. Du, F. Xiao, and X. Li, 2012. Subpixel land cover mapping by integrating spectral and spatial information of remotely sensed imagery, *IEEE Geoscience and Remote Sensing Letters*, 9(3):408–412.

Ling, F., X. Li, Y. Du, and F. Xiao, 2013. Sub-pixel mapping of remotely sensed imagery with hybrid intra- and inter-pixel dependence, *International Journal of Remote Sensing*, 34(1):341–357.

Ling, F., Y. Du, F. Xiao, H. Xue, and S. Wu, 2010. Super-resolution land-cover mapping using multiple sub-pixel shifted remotely sensed images, *International Journal of Remote Sensing*, 31(19):5023–5040.

Ling, F., Y. Du, X. Li, W. Li, F. Xiao, and Y. Zhang, 2013. Interpolation-based super-resolution land cover mapping, *Remote Sensing Letters*, 4(7):629–638.

Lu, D., M. Batistella, E. Moran, S. Hetrick, D. Alves, and E. Brondizio, 2011. Fractional forest cover mapping in the Brazilian Amazon with a combination of MODIS and TM images, *International Journal of Remote Sensing,* 32(22):7131–7149.

Lu, D., P. Mausel, E. Brondizio, and E. Moran, 2004a. Change detection techniques, *International Journal of Remote Sensing*, 25(12):2365–2407.

Lu, D., M. Batistella, and E. Moran, 2004b. Multitemporal spectral mixture analysis for Amazonian land-cover change detection, *Canadian Journal of Remote Sensing*, 30(1):87–100.

Makido, Y., and A. Shortridge, 2007. Weighting function alternatives for a subpixel allocation model, *Photogrammetric Engineering & Remote Sensing*, 73(11):1233–1240.

Makido, Y., A. Shortridge, and J.P. Messina, 2007. Assessing alternatives for modeling the spatial distribution of multiple land-cover classes at sub-pixel scales, *Photogrammetric Engineering & Remote Sensing*, 73(8):935–943.

Mertens, K.C., B. De Baets, L.P.C. Verbeke, and R.R. De Wulf, 2006. A sub-pixel mapping algorithm based on sub-pixel/pixel spatial attraction models, *International Journal of Remote Sensing*, 27(15):3293–3310.

Muad, A.M., and G.M. Foody, 2012. Super-resolution mapping of lakes from imagery with a coarse spatial and fine temporal resolution, *International Journal of Applied Earth Observation and Geoinformation*, 15:79–91.

Nguyen, M.Q., P.M. Atkinson, and H.G. Lewis, 2006. Superresolution mapping using a hopfield neural network with fused images, *IEEE Transactions on Geoscience and Remote Sensing*, 44(3):736–749.

Pontius, R.G., and M. Millones, 2011. Death to Kappa: Birth of quantity disagreement and allocation disagreement for accuracy assessment, *International Journal of Remote Sensing*, 32(15):4407–4429.

Roberts, D.A., M. Gardner, R. Church, S. Ustin, G. Scheer, and R.O. Green, 1998. Mapping chaparral in the Santa Monica Mountains using multiple endmember spectral mixture models, *Remote Sensing of Environment*, 65(3):267–279.

Shen, Z., J. Qi, and K. Wang, 2009. Modification of pixel-swapping algorithm with initialization from a sub-pixel/pixel spatial attraction model, *Photogrammetric Engineering & Remote Sensing*, 75(5):557–567.

Tatem, A.J., H.G. Lewis, P.M. Atkinson, and M.S. Nixon, 2003. Increasing the spatial resolution of agricultural land cover maps using a Hopfield neural network, *International Journal of Geographical Information Science*, 17(7):647–672.

Tolpekin, V.A., and A. Stein, 2009. Quantification of the effects of land-cover-class spectral separability on the accuracy of Markov-random-field-based superresolution mapping, *IEEE Transactions on Geoscience and Remote Sensing*, 47(9):3283–3297.

Tong, X., X. Zhang, J. Shan, H. Xie, and M. Liu, 2013. Attraction-repulsion model-based subpixel mapping of multi-/hyperspectral imagery, *IEEE Transactions on Geoscience and Remote Sensing*, 51(5):2799–2814.

Verhoeye, J., and R. De Wulf, 2002. Land cover mapping at sub-pixel scales using linear optimization techniques, *Remote Sensing of Environment*, 79(1):96–104.

Villa, A., J. Chanussot, J.A. Benediktsson, and C. Jutten, 2011. Spectral unmixing for the classification of hyperspectral images at a finer spatial resolution, *IEEE Journal of Selected Topics in Signal Processing*, 5(3):521–533.

Wang, L., and Q. Wang, 2013. Subpixel mapping using Markov random field with multiple spectral constraints from subpixel shifted remote sensing images, *IEEE Geoscience and Remote Sensing Letters*, 10(3):598–602.

Wang, Q., W. Shi, and L. Wang, 2014. Indicator cokriging-based subpixel land cover mapping with shifted images, *IEEE Journal of Selected Topics in Applied Earth Observation and Remote Sensing*, 7(1):327–339.

Wang, Q., L. Wang, and D. Liu, 2012. Particle swarm optimization-based sub-pixel mapping for remote-sensing imagery, *International Journal of Remote Sensing*, 33(20):6480–6496.

Xian, G., and C. Homer, 2010. Updating the 2001 National Land Cover Database impervious surface products to 2006 using Landsat imagery change detection methods, *Remote Sensing of Environment*, 114(8):1676–1686.

Xu, Y., and B. Huang, 2014. A spatio–temporal pixel-swapping algorithm for subpixel land cover mapping, *IEEE Geoscience and Remote Sensing Letters*, 11(2):474–478.

(Received 26 September 2013; accepted 11 August 2014; final version 26 August 2014)